USGS
science for a changing world

Prepared for the National Aeronautics and Space Administration

Geologic Map of the MTM –20272 and –25272 Quadrangles, Tyrrhena Terra Region of Mars

By Scott C. Mest and David A. Crown

Pamphlet to accompany
Scientific Investigations Map 2934

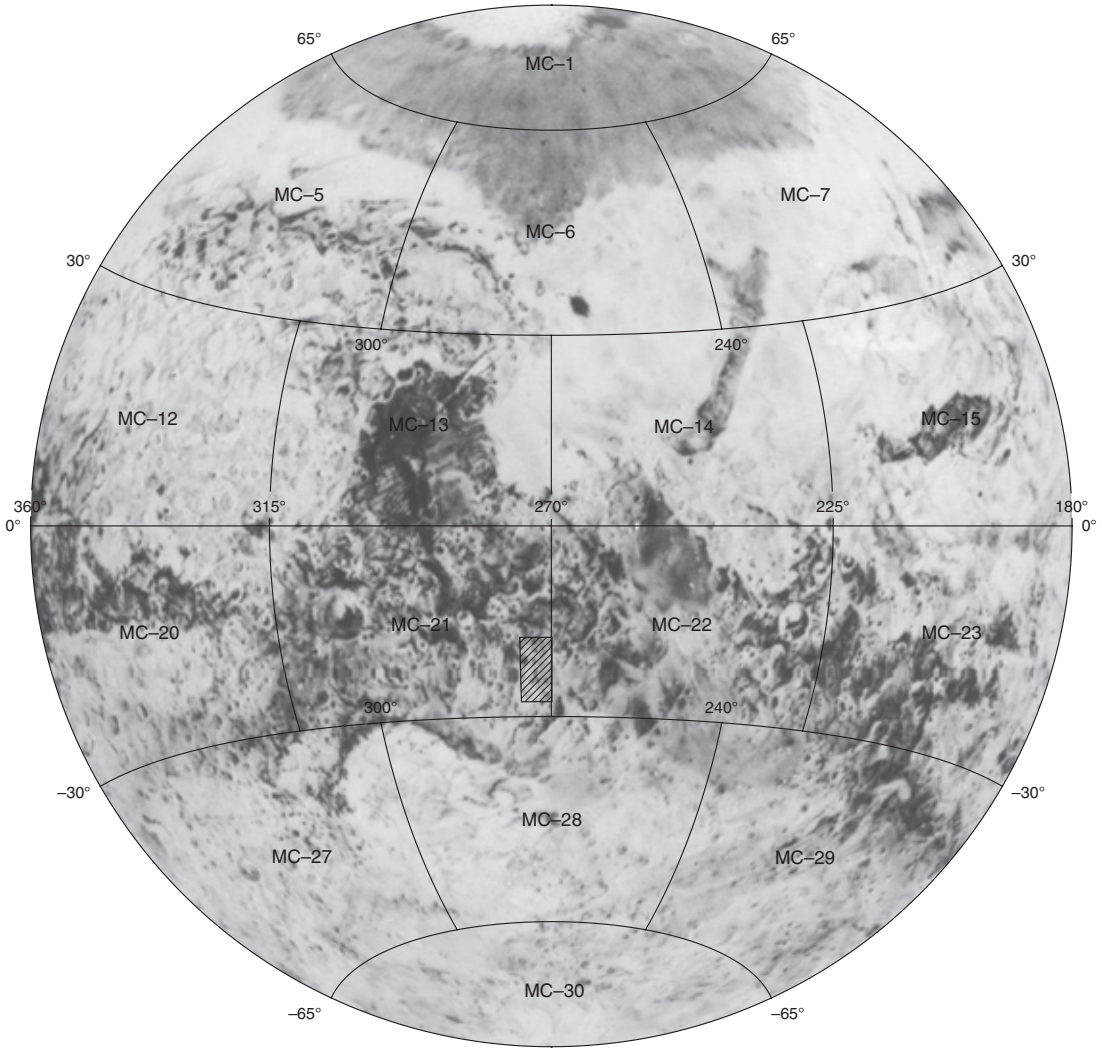

2006

U.S. Department of the Interior
U.S. Geological Survey

INTRODUCTION

Mars Transverse Mercator (MTM) –20272 and –25272 quadrangles (lat 17.5°–27.5° S., long 270°–275° W.) cover part of the highlands of Tyrrhena Terra north of Hellas Planitia (fig. 1). The surface of the Tyrrhena Terra region records a complex history of impact cratering and modification by fluvial and eolian activity (Schaber, 1977; Greeley and Guest, 1987; Craddock and Maxwell, 1993; Maxwell and Craddock, 1995; Tanaka and Leonard, 1995; Leonard and Tanaka, 2001; Mest and Crown, 2002a, 2005; Mest, 2004). The map area consists primarily of intercrater plains, impact crater material, and crater floor material (Mest and Crown, 2002a, 2005). An extensive valley network, Vichada Valles, as well as several smaller networks, dissects the northern part of the map area. The abundance and widespread nature of fluvial features within the map area have significant implications for past Martian environmental conditions. The degraded terrains surrounding Hellas Planitia provide constraints on the role and timing of volatile-driven activity in the evolution of the highlands (Mest and Crown, 2001a). The geologic history of this area may have been influenced not only by the presence of Hellas Planitia but also by other buried impact basins as described by Frey and others (2000).

REGIONAL GEOLOGY

The highlands surrounding Hellas Planitia include Noachian material that represents some of the oldest rocks on Mars (Murray and others, 1971; Tanaka, 1986; Tanaka and others, 1988, 1992). MOLA data show that the map area slopes approximately 0.23° S. toward Hellas Planitia and is surrounded by large impact craters and rugged highland material at higher elevations (fig. 2). Erosion of highland material characterized the Late Noachian Epoch and continued throughout the Hesperian Period, resulting in deposition of extensive plains materials in and around Hellas Planitia (Greeley and Guest, 1987; Crown and others, 1992; Leonard and Tanaka, 2001; Mest and Crown, 2001a). The geologic units along the north rim of Hellas Planitia were initially grouped into the plateau and high-plains assemblage, which consists of several rugged and cratered highland units and various younger plains units, some of which contain channels, ridges, scarps, and mesas (Greeley and Guest, 1987). Previous mapping at 1:5,000,000 (Schaber, 1977) and 1:15,000,000 (Greeley and Guest, 1987) scales each describe two main units in the highlands north of Hellas Planitia shown in this map: the "hilly and cratered highland material" and "dark mottled plains material" (Schaber, 1977) and the "dissected plateau material" and "ridged plains material" (Greeley and Guest, 1987). These researchers interpreted this area to be a mixture of volcanic material and ancient impact breccias and ejecta that represents a heavily dissected part of the highlands (Schaber, 1977; Greeley and Guest, 1987). Previous Viking-based analyses by Maxwell and Craddock (1995) in eastern Tyrrhena Terra (lat 15°–30° S., long 260°–270° W.) showed that formation of intercrater plains units, emplaced following extensive highland erosion, occurred in the Noachian Period. Erosion of impact craters and highland terrains in Tyrrhena Terra, as well as other equatorial (±30° lat) highland regions, resulted primarily from fluvial processes that were most likely precipitation driven (Craddock and Maxwell, 1993; Craddock and Howard, 2002).

Central-vent volcanism in the highlands surrounding Hellas Planitia occurred in the Late Noachian and Early Hesperian Epochs during formation of the highland paterae (Greeley and Crown, 1990; Crown and others, 1992; Crown and Greeley, 1993; Tanaka and Leonard, 1995; Gregg and others, 1998). Hadriaca and Tyrrhena Paterae, southeast and east of the map area, respectively, are interpreted to consist of pyroclastic deposits, possibly resulting from phreatomagmatic eruptions as magma rose through surface material containing ground ice or water (Greeley and Spudis, 1981; Greeley and Crown, 1990; Crown and Greeley, 1993). The presence of lava flow lobes within the approximately 1,000-km-long Tyrrhena Patera flowfield and a smooth deposit filling the caldera of Hadriaca Patera suggest that some effusive activity occurred late in the volcanic history, presumably during the Late Hesperian to Early Amazonian (Crown and others, 1992; Gregg and others, 1998; Mest and Crown, 2001b).

STRATIGRAPHY

Geologic units in MTM –20272 and –25272 quadrangles were identified and characterized using a combination of Viking Orbiter (VO), Mars Global Surveyor (MGS), Mars Orbiter Camera (MOC), and Mars Odyssey Thermal Emission Imaging System (THEMIS) images and Mars Orbiter Laser Altimeter (MOLA) and Thermal Emission Spectrometer (TES) data. We determined relative ages of geologic units using observed stratigraphic and crosscutting relations in combination with crater size-frequency distributions (table 1).

MAPPING METHODOLOGY

We analyzed the geologic units exposed in the Tyrrhena Terra region using VO, MOC, and THEMIS images, TES data, and MOLA topography. VO image coverage of the map area generally ranges from 150–170 m/pixel near crater Isil (south-central MTM –25272) to approximately 230 m/pixel; however, the west-central part of the map area, which includes Millochau crater, is covered by high-resolution VO images (~61 m/pixel). High-resolution MOC coverage (~2–6 m/pixel) is sparse in the map area but has proven useful in characterizing geologic material in detail, as well as analyzing the spatial extents of various units identified in the region. THEMIS daytime infrared (~95–100 m/pixel) and visible (~18–20 m/pixel) images cover much of the map area and provide adequate intermediate image resolutions to correlate units observed in both VO and MOC images. TES data (3 km/pixel) were used specifically to characterize the deposits on the floor of Millochau crater. MOLA topographic data were used to identify relations between valleys and impact craters, as well as to assess the distributions and stratigraphic positions of geologic units.

The unit color scheme used in this map follows that of Tanaka and others (2005). Color is used to provide relative age information for most units; a violet to red spectrum represents oldest to youngest units, respectively. However, the three units designated as other crater deposits (units c_3, c_2, c_1) do not follow this scheme because they are widespread both spatially and temporally within and outside of the map area, and they have no definitive Martian age.

CRATER COUNTING METHODOLOGY

We compiled crater size-frequency distributions to constrain the relative ages of geologic units and to determine the timing and duration of inferred geologic processes. Relative age information for the geologic units in MTM –20272 and –25272 quadrangles (1:500,000 scale; lat 17.5°–27.5° S., long 270°–275° W.) was partly derived by determining the number and size distribution of superposed impact craters for each geologic unit mapped (Tanaka, 1986). We digitized unit boundaries and determined unit areas using NIH Image 1.6 software. Individual craters were identified and counted using the MTM photomosaics and a Mars Digital Image Mosaic of VO images (MDIM 2; 231.4 m/pixel; lat 13°–30° S., long 265°–280° W.), as well as individual VO frames. Crater diameters were measured in centimeters using Adobe Illustrator 9.0 software and were converted to kilometers; diameters for larger craters were checked for accuracy using GRIDVIEW software (Roark and others, 2000; Roark and Frey, 2001).

The highland terrain of the map area contains impact craters of a wide range in size to a maximum of approximately 114 km in diameter. Based on VO images, the minimum crater diameter counted in valley floor material (unit HNvf), highland material (smooth plateau unit, Hpl_3; intercrater plains material, unit Npi; mountainous material, unit Nm), and crater floor material (unit HNcf) was 500 m. Craters with a diameter greater than 50 m were counted in talus material (unit AHt) and the Millochau floor deposits (dune, unit Amd; etched, unit HNme; rugged, unit HNmr; pitted, unit Nmp), incorporated from the detailed study of Millochau crater by Mest and Crown (2005), using a combination of VO, MOC, and THEMIS images. Only craters with a diameter greater than 3 km are shown on the map. Table 1 summarizes the crater size-frequency distribution data for the cumulative number of craters with diameters >2, >5, and >16 km/10^6 km^2 (N(2), N(5), N(16)) in each geologic unit mapped; crater size-frequency errors = ± (($N^{1/2}$) / A) × (10^6 km^2)) (Arvidson and others, 1979). The N(2), N(5), and N(16) data and their associated uncertainties were then compared for each unit and were used to determine the crater count age range (table 1). Determination of Martian unit ages (table 1) for the mapped units is based on crater size-frequency distributions combined with stratigraphic and cross-cutting relations; these ages are described in the text and Description of Map Units and shown on the Correlation of Map Units.

A consistent crater-counting methodology could not be applied to all units in the map area due to the limited areal exposure of some units and the presence of many large-diameter craters with widespread ejecta blankets associated with the related complicating effects of secondary craters. We found significant variation in the areal exposures of map units and the presence of large-diameter impact craters with distinct, widespread ejecta blankets that may superpose these units. Several units have small areas, specifically valley floor material (unit HNvf), talus material (unit AHt), mountainous material (unit Nm), and the Millochau crater floor deposits (units Amd, HNme, HNmr, Nmp). Valley floor material forms narrow linear deposits that typically do not show clear relative age relations to impact crater ejecta; however, an example of clear age relations occurs where the trunk valley of Vichada Valles appears to be truncated and partly buried by the ejecta from several large (>25 km diam) craters near lat 24° S. These craters have ejecta blankets that cover areas extending out to distances twice as large as their diameters. Where age relations are clear, craters with widespread eject blankets were not included in counts for units of small areal extent. To include these craters in the counts for valley floor material would also require including the areas of their ejecta blankets in the area of valley floor material. This would imply that large quantities of valley floor material presumably extend to some distance beneath the ejecta deposits; whereas, in reality, valley material would only account for a minor fraction of the surface buried by the ejecta. Inclusion of the area of the ejecta deposits with the area of limited-exposure units would greatly increase the areas of those units and provide inaccurate crater statistics and relative ages.

For units with large areas, such as intercrater plains (unit Npi), the method of counting all craters superposed on the surface does not present a problem. The plains are mapped as a widespread unit that has been superposed by a number of large-diameter impact craters. If a crater with widespread ejecta superposes plains material and this ejecta is even partly surrounded by plains material, it is reasonable to assume that plains material composes a large portion of the surface underlying the ejecta. In cases such as this, which are typical for large craters in the map area, these craters were counted and their areas were included in the area of the unit of interest.

An additional difficulty in interpreting crater size-frequency distributions is the potential that numerous secondary craters may be included in the crater counts. Definitive identification of secondary craters is difficult if not impossible. There are some clear identifiers of secondary craters, such as closely spaced chains, clusters of small-diameter craters, and elongated forms, that allow them to be excluded from the counts. Undefined individual secondary craters were potentially counted and included in our crater size-frequency distributions. Due to the inclusion of these craters, relative age estimates could be skewed to older ages. However, given the presence of numerous, large, fresh-appearing craters, every unit has the potential to contain secondary craters that may skew relative ages in a fairly uniform manner.

HIGHLAND MATERIAL

The oldest geologic unit exposed in the map area is mountainous material (unit Nm), which forms a few small knobs

believed to be the remnants of ancient crustal material uplifted during formation of impact basins and large craters (Scott and Tanaka, 1986; Greeley and Guest, 1987) and is surrounded by younger plains material and impact ejecta. Crater size-frequency distributions for unit Nm show ages ranging from Early Amazonian to Middle Noachian for N(2) (table 1). The degradational history, the especially small areal extent of unit exposures, and the small number of craters observed on mountainous material account for the anomalously young ages and, therefore, do not allow relative ages to be accurately determined from crater statistics alone. Morphologically, the knobs of mountainous material in the map area are similar in appearance to exposures in other parts of the Martian highlands and are most likely Middle Noachian in age, although regionally the unit began forming in the Early Noachian as a result of impact basin formation.

Impact craters and their ejecta cover much of the map area; about 30 craters larger than 10 km in diameter have preserved ejecta blankets typically approximately 30–50 km across and as much as 480 km across. The surrounding highland material, which was previously described by Greeley and Guest (1987), is classified as intercrater plains material (unit Npi) and the smooth plateau material (unit Hpl_3). Intercrater plains material contains well-integrated networks of fluvial valleys and exhibits a surface that was shaped predominantly by repeated impacts (fig. 3). In VO images, intercrater plains typically exhibit a smooth to irregular surface; closer investigation reveals that most irregularities within the plains result from a complicated mixture of crater material, such as ejecta blankets, that cannot be traced to specific source craters. Brightness changes very little across the surface of intercrater plains in both VO and THEMIS infrared daytime images except for subtle mottling or slight changes in gray scale, which are most likely due to the uneven distribution of ejecta and eolian deposits over the plains.

Both wide- and narrow-angle MOC images of the intercrater plains show a strikingly different surface than the one observed in VO images, due to higher spatial resolution and different illumination conditions. Wide- and narrow-angle MOC images show albedo changes that correlate with topography and may provide evidence for the redistribution of dust or dark sand. For example, areas of low topography, such as plains adjacent to incised valleys, generally display lower albedo than the adjacent topographic highs; from MOLA data, the differences in relief for these topographically low (dark) and high (bright) areas are typically no more than a few tens of meters. These albedo patterns also allow identification and detailed mapping of valley network systems. High-resolution MOC images of intercrater plains show many small (<1 km diam), poorly preserved craters that appear to have been eroded and (or) buried and are only visible as shallow rimless depressions (figs. 4, 5). The most heavily dissected intercrater plains material occurs in the northern part of the map area and is separated from a narrow strip of less dissected intercrater plains material to the south by a cluster of about 20 large (>10 km diam) craters. The northern exposure of intercrater plains material contains high concentrations of landforms we believe were formed by fluvial processes. The most obvious features are the numerous valleys that dissect the plains; the valleys tend to form dendritic or parallel patterns that are related to local topography. Networks on steep slopes, such as south of Millochau or along the rims of other craters, tend to form parallel patterns; whereas, networks within the more gradually sloping portions of the plains form open, dendritic patterns. In some of the larger valleys (Carr, 1995, 1996), the floor material may be discerned and mapped as a separate unit from intercrater plains material. In MOC images (fig. 5), the plains exhibit minor terracing where exposed along valley walls, indicating that the plains may consist of Noachian strata of various origins, such as impact material and breccias, volcanics, or sediments, or that the terraces may provide a record of past flow events.

The intercrater plains material contains an abundance of scarps, most of which are interpreted as erosional features, but some may also have tectonic origins or indicate the locations of buried and (or) eroded impact craters. High-resolution MOC images show that several low-relief scarps are oriented orthogonal to valleys and generally intersect valleys at angles similar to tributary valleys; these scarps may be erosional and provide evidence for undeveloped valleys. We also observe that the high-standing areas (fig. 4) generally consist of heavily pitted material that appears competent in nature; whereas, lower areas (floors of large pits, eroded craters, small tributaries) are infilled with dark sediments. Roughly 13 linear to arcuate ridges are also visible within the plains or are buried by crater ejecta. The ridges are scattered throughout the map area, and they do not appear to show any preferred orientation. The ridges are generally only a few tens of kilometers long, with the longest being approximately 50 km; all have degraded morphologies. They do not display crenulations along their crests, which are typical of mare-type wrinkle ridges (Strom, 1972; Lucchitta, 1976; Fagin and others, 1978; Phillips and Lambeck, 1980). No embayment relations are observed with intercrater plains material, indicating the ridges are composed of intercrater plains material. The ridges appear to be eroded tectonic landforms or were formed entirely by erosional processes. The degraded nature of the ridges and lack of embayment relations suggest that they formed after the plains were emplaced and were eroded at the same time as the intercrater plains.

Parallel channels and valley networks dissect intercrater plains material immediately to the east and south of craters Millochau and Jumla. These networks appear to be more finely integrated and preserve finer scale detail than the larger networks, such as Vichada Valles, that dissect most of the intercrater plains. MOLA topography shows that the plains along the south rim of Millochau are approximately 500 m higher in elevation and have steeper slopes (~1°) than the plains containing Vichada Valles, suggesting that this part of the plains most likely consists of eroded impact crater material from Millochau and Jumla.

In VO images, the intercrater plains south of approximately lat 24° S. appear significantly less dissected than the plains to the north (fig. 6). MOLA data show that the southern plains are also approximately 600 m lower in elevation than the northern plains. This elevation change occurs at roughly lat 24° S. where a cluster of about twenty large (>10 km diam) craters

stretches from east to west across the map area (fig. 2) and is traceable into adjacent quadrangles, such as MTM –25262 and –30267 quadrangles (Crown and Greeley, in press), where the highlands meet the volcanic deposits of the highland paterae. Red dots on the map show the locations of five MOC images (M01-02558, M11-03386, M18-01026, M22-02342, and E09-00634) that display the dune-covered nature of the southern part of the map area, which is not visible at map scale. MOC images show an abundance of dune features on the surface of this part of the intercrater plains (fig. 7), as well as on impact crater ejecta (M22-02342); however, small areas of the pitted and cratered surface diagnostic of the intercrater plains material in the northern part of the map area are visible among the dunes. This suggests that the intercrater plains material is quite extensive and appears to have been modified by fluvial processes, as well as buried in some areas by impact ejecta and wind-blown material. Greeley and Guest (1987) previously mapped the southern part of the intercrater plains as ridged plains material, although only 5 of the 13 ridges identified in the plains are found in this part of the map area, and almost all of those are completely to partially buried by impact ejecta. This part of the map area does not show the high density of wrinkle ridges typical of Hesperian ridged plains material. No lava flow features are visible within this unit in the map area.

Intercrater plains material (unit Npi) is similar to the dissected plateau material of Greeley and Guest (1987), consisting of sequences of impact breccias, volcanic deposits, and sediments deposited early in the region's history and covered in many places by ejecta from nearby craters. Erosion by fluvial processes produced extensive networks of valleys that dissected the plains and resulted in a variety of landforms. Portions of the plains observed in MOC images show that the upper few meters of material have been removed; small pockets of smoother, dark material fill low-lying areas as the heavily pitted surface is removed. Eolian activity has since buried the topographically lower southern portions of the plains and resulted in the formation of dunes.

Crater size-frequency distributions for intercrater plains material show ages ranging from Early to Late Noachian. Superposition relations between craters and the plains are difficult to determine for many of the larger degraded craters, where there is little to no ejecta preserved or the ejecta grades into the surrounding plains. Based on the dissected nature of the plains and observed variations in the distribution of fluvial valleys, we believe that nonadjacent craters of similar size could also be of similar age despite significant differences in their preserved state. Morphologic differences could be due to underlying lithology, the characteristics of the ejected material, and the nature of the erosional process(es), any of which might result in different levels of resistance to erosion. Our interpretation that intercrater plains material consists of interlayered deposits of impact material, volcanic deposits, and sediments that have been eroded by fluvial processes suggests a long history of emplacement. N(2), N(5), and N(16) crater statistics (table 1) show relations between valley floor deposits and the intercrater plains that are consistent with crosscutting relations, indicating that valley floor deposits are younger than the adjacent intercrater plains material. Formation of the plains may have begun in the Early Noachian, but emplacement of most of the unit occurred during the Middle and Late Noachian Epochs.

The smooth plateau unit (Hpl3; defined by Greeley and Guest, 1987) is exposed in the southeast corner of the map area. This unit was initially mapped as "dark mottled plains material" by Schaber (unit pdm, 1977) and "ridged plains material" by Greeley and Guest (unit Hr, 1987); recently the smooth plateau unit was mapped in adjacent quadrangles by Crown and Greeley (in press). Unit Hpl3 shows a smooth surface with a few wrinkle ridges and some channels that occur at the base of a scarp that forms the contact with the intercrater plains. Based on geologic mapping by Crown and Greeley (in press) in MTM –30267, the smooth plateau unit is composed of Hesperian-aged volcanic deposits and sediments, although there are no flow features visible in this map area.

N(2) and N(5) crater size-frequency distributions (table 1) for the smooth plateau unit show ages of Late Noachian and Middle Noachian, respectively. The exposure of this unit in the map area suggests older ages than shown by global mapping studies (Greeley and Guest, 1987). Based on crater statistics determined for exposures of the smooth plateau unit in adjacent quadrangles (Crown and Greeley, in press), this unit is Early to Late Hesperian in age. The anomalously high number of craters on unit Hpl3 in the map area could be due to secondary craters associated with Isil at the south margin of the map and other large craters in the region.

VALLEY MATERIAL

Valley floor material (unit HNvf) appears to fill most of the valleys in the map area. These deposits are observed, and have been mapped, in the wider valleys based on characteristics in VO and MOC images; however, similar deposits are also believed to extend into smaller tributaries whose floors cannot be studied with the available image resolution. Valley floor material appears smooth to pitted in VO images. High-resolution MOC images show sediments that were mobilized to form dunes (fig. 5); individual dune outcrops are not mapped but are incorporated into valley floor material. The dunes are oriented perpendicular to the valley walls (transverse to the proposed direction of fluid flow within the valleys), and most of the larger dunes extend across the width of the valley; dune wavelengths range from 20 to 110 m (average ~50 m). From visual inspection of the dunes, it appears the backslopes of most dunes are oriented upstream, suggesting the dunes are most likely transverse dunes with wind directions oriented downstream. Numerous small craters are buried by valley floor material; however, MOC images (figs. 5*B*,*C*) show that several small craters also superpose dunes. Most craters that superpose dunes are small (<1 km diam) and ejecta deposits are difficult to observe, but figure 5*B* shows two craters with ejecta that appears to drape dunes. Figure 5*C* shows examples of a crater that bisects a dune, as well as similarly sized craters that are embayed by dunes. These relations help to constrain the age of the floor deposits, as well as the timing of fluid flow through the valleys. Craters superposing dunes suggests that

the dunes are relatively stable and may indicate that either (1) the sediments that compose the dunes are difficult to mobilize, (2) the wind velocities required to form dunes within the valleys are no longer present, and (or) (3) the craters stabilized portions of active dunes.

We interpret valley floor material to consist of sediments derived from the surrounding highland material that was deposited by a combination of water flowing through the valleys, mass-wasting of valley walls, and eolian processes. Crater size-frequency distributions (table 1) for valley floor material show ages ranging from Early to Late Noachian. Crosscutting relations with intercrater plains material indicate that valley floor material must be younger than the plains material; therefore, valley floor material is Late Noachian or younger, which is consistent with N(2) and N(5) distributions. It is also possible that different exposures of valley floor deposits are significantly different ages, spanning from Noachian to Amazonian Periods.

CRATER MATERIAL

Crater material within the map area displays various states of preservation presumably resulting from different combinations of crater age, target lithology, and erosional environment, though crater morphology in general implies progressive degradation throughout the evolution of this region. Well-preserved crater material (unit c_3) shows the least amount of degradation and is characterized by pronounced, continuous crater rims that are elevated relative to the surrounding materials and also by well-defined, continuous ejecta blankets. Numerous clusters and chains of small craters are observed within unit c_3 ejecta blankets and are likely secondary craters. Moderately degraded crater material (unit c_2) is characterized by crater rims that may be discontinuous, exhibiting minor relief above the surrounding material, and by discontinuous and (or) poorly exposed ejecta blankets. Highly degraded crater material (unit c_1) shows discontinuous crater rims exhibiting little to no relief above the surrounding material, ejecta blankets that were either eroded or mantled by younger material, or some combination of the two. The abundance of large highland craters with distinct ejecta material allows us to determine superposition relations between adjacent craters. In some cases, ejecta material of similar preservation state cannot be traced to specific source craters and is mapped as single, large exposures containing several source craters. Martian ages are not formally assigned to impact crater material, but crater size-frequency distributions on three sample areas for c_3 (crater Isil; lat 27.2° S., long 272.1° W.), c_2 (lat 20.3° S., long 271.7° W.) and c_1 (lat 19.6° S., long 273.3° W.) craters show relative ages of Early Hesperian or younger, Middle Noachian to Early Hesperian, and Early to Late Noachian, respectively.

Many craters (units c_3, c_2, c_1) have smooth, flat floors and contain crater floor material (unit HNcf) while still retaining the original characteristic crater morphologies. Floor material may have various origins and, therefore, ages, which makes the presence or lack of this deposit an inappropriate method of characterizing craters within the map area. Ejecta blankets were modified to various degrees by fluvial processes, providing significant crosscutting relations to constrain the timing of fluvial activity. Several craters in Vichada Valles (fig. 8, craters a, b) may have ejecta blankets dissected by valleys, although it is difficult to determine whether or not ejecta is present on the valley floors.

Many of the impact craters in the map area display low-relief rims and flat, relatively smooth floors; these craters contain distinct deposits that are mapped as crater floor material (unit HNcf). Crater floor material is also mapped in some craters that have less-degraded morphologies. Some crater interior deposits, such as those in Millochau, are mapped in more detail than other craters due to the availability of larger scale coverage by MOC and THEMIS images (Mest and Crown, 2005). MOC image E16-01803 shows that crater interior deposits within a 36-km-diameter crater, located at lat 23.5° S. and long 273.5° W. (fig. 9), consist of several distinct layers that are in the process of being eroded, exposing what appears to be the remnants of a cratered plateau and buried impact craters. The very bright material surrounding the plateau (fig. 9) could consist of material deposited in a shallow lake.

Some crater floor deposits display lobate margins; whereas, others terminate gradually against the interior crater walls. Most of the filled craters have gullied interior walls, which suggest that some of the crater floor material consists of debris eroded from the crater walls and deposited on the crater floor. Some craters were breached by valleys (fig. 3), indicating that a part of these deposits is most likely derived from material eroded from the surrounding highlands. Some exposures of crater floor material may be lacustrine in origin, resulting from standing bodies of water contained in crater interiors. Also, some component of crater floor material may be composed of eolian deposits, derived both locally and regionally. Previous studies of highland terrains (Grant and Schultz, 1993, 1994; Crown and Stewart, 1995; Grant, 1999; Mest and Crown, 2001b; Pierce and Crown, 2003) show that mass wasting of crater rim and wall materials can contribute significant amounts of material to crater floors. Although no evidence for discrete mass movements, such as lobes of debris extending from crater walls or transverse or longitudinal ridges, is observed on crater floors in this map area, some contribution from mass wasting is likely. Deposits of crater floor material contain few large craters on their surfaces, but the moderately low total surface area of these units yields relatively high crater densities. Crater size-frequency distributions (N(2), N(5), N(16)) of crater floor material suggest that these deposits are Middle Noachian to Late Hesperian in age. Eolian deposition within craters would result in burial of many small craters, skewing crater floor material toward younger ages. In addition, exposures of crater floor material with significantly different ages (Noachian to Amazonian) may be present in the map area.

Millochau, centered at lat 21.4° S., long 275° W. (fig. 10), is approximately 114 km in diameter and, based on MOLA data, is approximately 2 km deep. The floor of the crater shows a variety of terrains that record a complex geologic history. Millochau contains four distinct deposits, mapped as Millochau dune (unit Amd), etched (unit HNme), pitted (unit Nmp), and rugged (unit HNmr) materials. Six high-resolution MOC

images are available that allow these deposits to be identified and characterized separately from the crater floor material (unit HNcf) that fills other large craters in the map area. Seven THEMIS visible (two images) and infrared (four daytime IR and one nighttime IR) images provide almost complete coverage of Millochau's rim and interior deposits (Mest and Crown, 2005). Analysis of MOC and THEMIS images reveals numerous small exposures of these units in close proximity that are shown at map scale. Mest and Crown (2005) provide a detailed analysis of the Millochau floor deposits as part of a study to characterize crater interior deposits and their relation to regional geologic evolution.

The floor of Millochau contains a plateau northeast of the crater's center that is raised as much as 400 m above the surrounding floor. This plateau is bounded on its north and east edges by a scarp and a series of irregular depressions; the plateau slopes gently to the south and west where it grades into the surrounding deposits (fig. 10). Numerous layers are exposed along the scarp boundary of the plateau, as well as along knobs and mesas found in the depressions. These layers vary in thickness and are traceable across tens of kilometers in MOC images; outcrops observed in MOC images tend to exhibit a regular sequence of layering with a thick (150–250 m) and relatively massive layer overlying several thin (<10 m) layers (Mest and Crown, 2005). Martian craters of Millochau's size exhibit complex interiors (Wood, 1980; Pike and Spudis, 1987); however, the size and position of the plateau in the north central part of the crater floor combined with the presence of layering, exposed in knobs and outcrops of the plateau, suggest that this feature is primarily a secondary feature unrelated to the Millochau impact event (Mest and Crown, 2005). The south edge of the plateau contains several valleys, oriented roughly north-south, that cut into the plateau. These valleys have fairly consistent widths and depths and they display amphitheater-shaped heads suggesting that they formed primarily by collapse and groundwater sapping. Similar but smaller valley-like features cut into the north-facing scarp of the plateau and the south-facing scarp of the surrounding floor material. Valleys in the plateau tend to be contained entirely within the plateau.Where the valleys meet the Millochau rugged material along the south edge of the plateau, the mouths of the valleys terminate at the contact with the Millochau rugged material, suggesting that there was little to no downcutting into the rugged material.

Millochau pitted material (unit Nmp) is found only on the central plateau and shows a heavily pitted and cratered surface (fig. 11) in MOC images. Portions of this unit display subtle brightness variations in THEMIS images that correlate to surfaces exhibiting differences in degradation and possible mantling by ejecta from a 23-km-diameter crater in western Millochau (Mest and Crown, 2005). Dark surfaces appear more rugged and contain more craters and pits than light surfaces. Light surfaces are rugged as well, but the craters and pits are more pristine. Light surfaces also appear to be higher standing, suggesting this material may be in the process of being eroded to expose the underlying darker material, or low areas may contain a lag deposit or coarse sand. Although dark pitted material appears to contain more craters than the light material, the size ranges of craters are similar for all pitted material. TES thermal inertia data for Millochau pitted material ranges from approximately 275 to 350 J/m^{2}Ks$^{1/2}$ and corresponds to surface material that contains fine material and (or) few rocks (Jakosky and others, 2000; Mellon and others, 2000; Christensen and others, 2001; Putzig and others, 2003). THEMIS infrared images also show Millochau pitted material is bright during the day and dark at night, suggesting this unit consists of fine-grained deposits that heat and cool relatively quickly. The presence of many small (<1 km diam) impact craters in the map area is similar to cratering in the northern intercrater plains and suggests these units may be similar in age. Millochau pitted material may be composed partly of sedimentary deposits but may also contain components of volcanic material and impact-related (ejecta, impact melt) deposits that extended across nearly the entire floor of Millochau and were subsequently eroded. Capping the plateau, Millochau pitted material is topographically separated from the surrounding floor material by nearly 400 m of relief. This separation, combined with the morphologic expression of its surface and TES and THEMIS data, makes it distinct from other units within Millochau. It is possible that some of the layering within the plateau that includes the pitted material could be lacustrine in nature, suggesting that Millochau may have contained large standing bodies of water. Pits on the surface of the deposit could be due to a large number of poorly preserved impact craters, collapse features, and (or) wind-modified depressions. Scarps within the deposit are most likely erosional and may indicate the locations of immature sapping valleys (Mest and Crown, 2005).

Millochau rugged material (unit HNmr) forms irregular surfaces that exhibit a stucco-like texture (figs. 12, 13) and slope approximately 0.8° from the base of the interior wall down to the central plateau. Most craters are poorly preserved, showing highly degraded rims and little to no ejecta. Low areas within the unit typically contain dune material. High-resolution (8–11 m/pixel) VO images show low-relief (<20 m) scarps cutting through rugged material in the southern and eastern parts of Millochau; further analysis of THEMIS visible and daytime infrared images reveal that these are not scarps but mare-type wrinkle ridges (Mest and Crown, 2005), which are likely tectonic (Strom, 1972; Lucchitta, 1976; Fagin and others, 1978; Phillips and Lambeck, 1980). Millochau rugged material appears to embay Millochau rim material where they are in contact, such as in the southwestern part of Millochau, but the embayments are not pronounced. Most of the rugged material that is presumably in contact with Millochau rim material is buried by talus in the north, the east, and parts of the south and by impact ejecta from Okotoks (MC–21, west of map area) in the south and west. Millochau rugged material near the base of the east wall appears in MOC image R04-01308 (fig. 13) to have been exhumed as overlying talus material was removed. Millochau rugged material exhibits TES-derived thermal inertia values of ~400–500 J/m^{2}Ks$^{1/2}$, suggesting rocky and (or) coarse-grained surface material or cemented fine material (Jakosky and others, 2000; Mellon and others, 2000; Christensen and others, 2001; Putzig and others, 2003). THEMIS

infrared images show that Millochau rugged material is dark during the day and bright at night, suggesting that the material that makes up this unit retains heat. The irregular surface of Millochau rugged material suggests that this unit experienced significantly more degradation or is less resistant to erosion than adjacent Millochau pitted material. The precise nature of Millochau rugged material is unclear, but we interpret it to be sedimentary (fluvial, playa, eolian), volcanic, and impact-related (ejecta, impact melt) deposits; the slope toward the crater center suggests it may be emplaced by mass wasting.

Millochau etched material (unit HNme) forms much of the terrain within the depressions that border the northern and eastern portions of the central plateau (figs. 11, 12). Unit HNme displays a variety of surface textures (smooth, lineated, irregular) and brightness variations and encompasses surfaces not incorporated within other units mapped in Millochau. MOLA data show that Millochau etched material is consistently topographically lower than pitted material but is found above and below rugged material (Mest and Crown, 2005). Some exposures of Millochau etched material are found within the depressions surrounding the plateau at roughly the same elevation as Millochau rugged material and may be eroded outliers of rugged material. Few fresh craters are observed within Millochau etched material; some exposures appear to contain craters that are being exhumed. Lineated Millochau etched material (fig. 11) shows polygons filled with bright and dark materials that are separated by narrow flat-topped ridges. It is unclear what material forms this surface, but one possibility is a thin layer that has been partially eroded. Lineated and irregular exposures of Millochau etched material are interpreted to be exhumed crater interior deposits; the thin layers observed in figure 11 suggest these deposits are sedimentary. Smoother exposures of Millochau etched material consist of eroded crater interior material redistributed via fluvial and eolian processes and may be unconsolidated to loosely consolidated. Collapse of overlying material and (or) erosion (fluvial and eolian) are probably the main processes operating to expose these deposits.

Millochau dune material (unit Amd) occurs in isolated patches that fill low-lying parts of pitted and etched materials (figs. 11, 12, 14). The material that forms these deposits is generally darker than the underlying material and forms long- and short-wavelength dunes, similar to those described by Edgett (2001a,b). We measured dune wavelengths on high-resolution MOC images and found 34 long-wavelength and 21 short-wavelength dunes. The long-wavelength dunes (~40–170 m; average ≈70 m) tend to be oriented east-west (long axis), and many span the widths of the depressions in which they occur. Short-wavelength (~10–30 m; average ≈20 m) dunes are shorter (long axis) and narrower than long-wavelength dunes. Short-wavelength dunes tend to be oriented parallel to the long-wavelength dunes, but some are perpendicular to and found between long-wavelength dunes; they are also typically oriented perpendicular to the dips of slopes of topographic highs (knobs and scarps). From MOC images, it appears that most short-wavelength dunes superpose the long-wavelength dunes, indicating that they are younger and more mobile. We interpret Millochau dune material to consist of sediments eroded from other interior floor deposits, as well as crater wall and rim material, and redistributed within low-lying areas by wind.

The materials that form the Millochau floor deposits have small areal extents and contain few large craters on their surfaces. The corresponding large statistical uncertainties suggest limited use of relative age determinations for these units. Crater size-frequency distributions for Millochau rugged, pitted, and etched materials do not allow identification of a distinct progression in age for these units. Stratigraphic relations between Millochau pitted and rugged material are unclear. But rugged material appears to embay the pitted material in some places, suggesting it is stratigraphically younger, and crater counts reflect formation age. Alternatively, rugged material could have been exposed when the plateau was eroded, yielding a younger surface than pitted material, and the crater counts reflect surface retention age. Millochau pitted material shows higher crater densities for craters 2, 5, and 16 km in diameter and is interpreted as Middle to Late Noachian in age. Millochau rugged material shows lower densities (N(2) and N(5)), consistent with its more degraded appearance and the potential for more crater obliteration than the pitted material, and is interpreted as Middle Noachian to Late Hesperian in age. If Millochau pitted material did overlay Millochau rugged material, it would have effectively shielded the rugged material from impacts while it continued to accumulate impacts. Removal of Millochau pitted material to its current extent, combined with erosion of Millochau rugged material and redistribution of sediments within this unit (and removal of small diameter craters), would yield the slightly younger ages that we observe (Mest and Crown, 2005). The age determination for Millochau rugged material may be more representative of its exhumation and modification rather than its emplacement, which could be closer to Middle Noachian. However, the margin of the plateau, which is the contact of pitted material with rugged material, appears degraded and irregular in the available THEMIS images, and the possibility of rugged material embaying pitted material cannot be discounted.

Determination of an age for Millochau etched material is difficult, because only two craters with diameters greater than 2 km were identified in the image data sets. Given our interpretation that Millochau etched material is composed of a combination of old exhumed surfaces and younger redistributed unconsolidated debris, these data may more accurately represent surface retention ages rather than stratigraphic ages. Age determination for Millochau etched material is based on superposition relations with Millochau pitted, rugged, and dune materials. The base lithology composing the irregular, knobby, and lineated outcrops of Millochau etched material likely formed a continuous surface that presumably extends beneath Millochau pitted and rugged materials. These exhumed materials are most likely Middle Noachian in age and older than Millochau pitted and rugged material; the depositional surfaces (smooth areas) formed after exhumation and could be as young as Late Hesperian, and their age is constrained by overlying Millochau dune material. As with Millochau rugged material,

the age designated for Millochau etched material represents a highly modified surface consisting of a mixture of reexposed older deposits and younger erosional debris. Millochau dune material contains no superposed craters greater than 0.5 km in diameter and is, therefore, Amazonian in age.

Okotoks crater (22.6 km diam), in western Millochau, displays a well-defined ejecta blanket (Mest and Crown, 2005) that superposes Millochau rim, pitted, and rugged materials. Crater size-frequency distributions for Okotoks (see Mest and Crown, 2005) suggest an age of Middle to Late Hesperian, thus providing an upper age constraint for these units, as well as for plateau formation and erosion. The ejecta from Okotoks appears relatively unmodified by the erosional processes that affected the pitted and rugged material, suggesting that emplacement and most of the erosion of these units occurred prior to formation of Okotoks within a window ranging from Middle Noachian to Late Hesperian.

Talus material (unit AHt) forms narrow deposits along the interior walls of Millochau, Jumla, and a large unnamed crater (lat 17.2° S., long 269.8° W.) and generally overlies crater floor material. These deposits are featureless in VO images but show significant detail in MOC image E04-02035 (fig. 15), which covers the part of Jumla crater that adjoins the Millochau east rim (fig. 10). In figure 15, surfaces a and b contain many recognizable craters despite a heavily degraded appearance, and portions of this surface resemble rugged material observed in Millochau that display irregular and degraded stucco-like surface textures. Figure 15 shows four distinct surfaces that were subjected to different amounts of erosion, and it appears that surfaces a, b, and possibly d are being eroded to reveal underlying surface c. From this image, it appears that the deposit shown in figure 15 at the base of the crater wall is layered, suggesting that this particular deposit of talus could consist of sequences of material deposited in several mass-wasting events. Talus material is interpreted to consist of unconsolidated debris shed from crater wall and rim material by mass wasting and deposited along the interior walls of craters. The surface texture suggests talus material may have been extensively eroded in a manner similar to rugged material. Few large craters are observed on deposits of talus material, which show ages of Late Noachian to Late Hesperian for N(2) crater distributions. The low number of craters combined with the small surface area of this unit results in large age uncertainties. Because talus material superposes crater floor material and Millochau rugged material, which are defined as Hesperian to Noachian in age, talus material most likely has an age that is Late Hesperian or younger. Although only three exposures of talus material are visible at map scale, smaller deposits of talus occur in other craters.

FLUVIAL FEATURES

The geologic evolution of the map area appears to have been greatly influenced by fluvial processes. The map area is dissected by large and small valley networks that display dendritic to subparallel patterns. The largest network, Vichada Valles, extends through much of the intercrater plains southward to the grouping of large craters at lat 24° S. and has tributaries that reach outside of the map area. The drainage basin enclosing Vichada Valles, as well as several of the smaller valley networks, occupies an area of approximately 300,000 km^2 and is elongated in a north-south direction (Mest, 2004; Mest, unpub. data, 2006). In MOLA data, the basin exhibits roughly 4.5 km in relief with a maximum elevation near 3.5 km and a minimum near –1.0 km. At some time in the past, Vichada Valles presumably debouched into Hellas Planitia, but evidence of this extension has been obscured by later events. Most tributaries of Vichada Valles head within an elevation range of approximately 1.5 to 2.5 km.

Most of the valley networks in the map area display highly degraded morphologies (figs. 3, 8). MOC images reveal that valleys have rounded banks, display terracing along valley walls, and have dunes covering their floors (fig. 5). MOLA profiles show that most trunk valleys have fairly flat or gently sloping floors and many tributaries are v-shaped in cross section. Valley depths range from approximately 70 to 200 m and widths range from approximately 0.9 to 10.5 km. Within the map area, the trunk valley of Vichada Valles branches and rejoins downstream several times along its length (fig. 3). Carr (1995, 1996) described one example of this phenomenon, attributing it to headward erosion of a sapping-type valley, where random headward extension led to intersection of the valleys upstream. However, the valley widths and depths change significantly along their lengths, which suggests another process of formation may be involved. In general, the larger valleys in the map area tend to vary in width along their lengths, possibly indicating areas of lateral flow or meandering, which is not characteristic of sapping-dominated valleys (Carr, 1995, 1996; Goldspiel and others, 1993; Goldspiel and Squyres, 2000).

Valleys and subparallel valley networks observed south of Millochau and east of the map area are smaller and appear less incised than Vichada Valles and other large valley networks. The tributaries of these smaller systems typically head at crater rim crests, at elevations between 1 and 2 km, and they are generally not more than a few hundred meters to a few kilometers long. The occurrence of these systems on steep slopes results in more closely spaced, first-order tributaries. The valleys south of Millochau either merge with intercrater plains material with no sign of deposition at their mouths or they are truncated by craters and buried by ejecta. Some of the smaller networks east of the map area empty into an old buried crater basin that has subsequently accumulated large impact craters on its floor. None of these smaller networks are observed to intersect Vichada Valles (Mest, 2004; Mest, unpub. data, 2006). The morphologic differences between these smaller networks and Vichada Valles could be due to differences in age, lithology, and (or) slope. In a synopsis by Carr (1995, 1996), the smaller and denser valley networks just east of the map area were not attributed to sapping alone, because many valleys head at crater rim crests; he suggested that some component of surface runoff was required to form these valleys, perhaps by overflow of craters that were filled to their rims with percolating groundwater combined with mass wasting of water-saturated material.

Identification of clear crosscutting relations between fluvial valleys and impact craters is difficult due to coverage by low-resolution VO images of much of the map area. Much of the dissection of the local plains material appears to have been contemporaneous with or postdate impact crater formation. For example, several of the moderately degraded craters in the northern and east-central parts of the map area have ejecta dissected by well-incised valleys (fig. 8). A valley dissects the terrain between two fairly pristine craters (fig. 8, craters a, b) in the northeastern part of the map area. VO images do not clearly resolve whether impact ejecta is found on the floor of this valley, but MOLA profiles across the valley show very little difference in its depth where the valley crosses the ejecta compared to upstream and downstream from the ejecta. It is also possible that any ejecta on the valley floor(s) was removed by subsequent flow events or redistributed by eolian processes.

Impact craters exhibiting breached rims are also observed in the map area but are not common. Two of the more prominent examples of breached craters are found at lat 20.7° S., long 273.1° W. (fig. 3, crater a) and lat 17.7° S., long 272.5° W.; although the second example is not mapped as an impact crater, its circular morphology suggests this feature is a crater that has been severely degraded, moreso than most degraded craters in this area. The first crater (fig. 3) displays a relatively flat interior containing several small impact craters, an inlet valley breaching the west rim, and an outlet valley breaching the southeast rim. Interpretation as a sequence of fluvial erosion and deposition is based on the morphologies of the inlet and outlet valleys. MOLA data show that the mouth of the inlet valley is approximately 200 m wider and 50 m deeper than the head of the outlet valley (widths: 1,100 m and 900 m; depths, 100 m and 50 m, respectively) and that the floor of the outlet valley is approximately 100 m higher in elevation than the floor of the inlet valley. These differences suggest that the inlet valley may have breached this crater first, resulting in ponding of water and deposition of sediments eroded from the surrounding highlands. The smaller outlet valley suggests that its incision probably did not occur until this crater was filled with water that overtopped the crater rim and began downcutting. There is no clear evidence, such as shorelines or benches, in available images of this crater to indicate water level; therefore, it is also possible that the outlet valley grew headward from the southeast until intersecting and breaching the crater rim. The rivers that breached both these craters likely carried material eroded from upstream exposures of intercrater plains and impact materials; the interiors of these breached impact craters, therefore, should contain a suite of fluviolacustrine deposits representative of the local highlands.

Impact craters that superpose valleys show that some large craters postdate valley formation and that there was little to no flow following the impact. For example, some craters that intersect valley segments do not cause visible damming and (or) diversion of water upstream by the structure of the crater or emplacement of its ejecta within the valley. If significant flow within these valleys was present at the time of impact, some evidence for ponding and deposition of sediments or for diversion of water and incision of a new channel should be present. Figure 8 shows a possible example for diversion of flow around a crater with no evidence for ponding upstream. These features are rarely visible in the available data sets.

Visible relations between valleys and other features in the map area suggest that valley network formation occurred prior to the majority of large impact craters. Combined with crater size-frequency distributions for valley floor material, this indicates that most of the valley formation in this part of the highlands was relatively old and that most fluvial activity ceased in the Late Noachian to Early Hesperian. Geologic mapping by Maxwell and Craddock (1995) in Tyrrhena Terra (lat 15°–30° S., long 260°–270° W.) showed similar results. In their study, dissected highlands and intercrater plains ranged from Middle to Late Noachian and Late Noachian to Early Hesperian in age, respectively, and dissection of these materials occurred in the Late Noachian to Early Hesperian.

Previous researchers (Carr, 1995, 1996) interpreted highland valleys, such as those in the map area, to have formed by combinations of surface runoff-induced mass wasting and sapping processes. However, questions regarding the ability of sapping to be sustained in local environments, such as along crater rims, have been raised (Craddock and Maxwell, 1993; Maxwell and Craddock, 1995). Furthermore, the ability to sustain an interconnected aquifer system in the highlands might be problematic over regional scales where the subsurface material may not be conducive for groundwater flow. Hydrologic modeling is currently being used to examine these problems to further constrain the fluvial evolution of the Tyrrhena Terra region (Mest and others, 2002; Mest, 2004; Mest, unpub. data, 2006).

GEOLOGIC HISTORY

Geologic mapping in the Tyrrhena Terra region of the Martian highlands reveals a surface that is significantly degraded and modified by impact, fluvial, and eolian processes. Most of the material is very old, ranging from Middle Noachian to Early Hesperian in age. Only surficial deposits, such as the limited exposures of dune material and talus show evidence for activity in the Amazonian Period. Mapping shows complex relations between impact craters and the valley networks that dissect the intercrater plains. Lack of consistent high-resolution coverage across the entire map area complicates interpretation of age relations; however, stratigraphic relations combined with crater size-frequency distributions provide general constraints on the geologic evolution of the map area.

Dominant events in the geologic development of this part of the highlands north of Hellas Planitia include the formation of Hellas Planitia and other large basins early in Mars history. The impacts forming these basins deposited ejecta over much of the surface and altered the topography of the highlands, forming large, low-lying areas that later collected sediments. During the Early and Middle Noachian Epochs, widespread intercrater plains formed by accumulation of some combination of sedimentary (fluvial and eolian), volcanic (may include flow sequences and (or) pyroclastic deposits), and impact-related (melt and ejecta) materials. These materials are layered, but

not consistently, across the highlands in the map area. The lack of evidence for volcanic flow features and the eroded nature of the plains material suggest that the uppermost layers most likely consist of sedimentary and impact deposits.

Heavy bombardment during the Noachian Period produced numerous (28) large (>10 km diam) impact craters, including Millochau, in the map area. At the same time, fluvial processes shaped the intercrater plains, forming well-incised networks of valleys and degrading the surfaces of plains, as well as cross-cutting ejecta deposits of some craters. As fluvial activity waned, numerous impacts continued to affect Tyrrhena Terra, which is shown by craters that truncate and (or) bury valley segments, such as the cluster of several large craters at about lat 24° S. These craters did not cause redirection of flow or ponding of water and sediments, indicating there was little to no flow within these channels at the time of impact. The nature of the fluvial activity that formed extensive valley networks has been questioned in this and other areas of the highlands (Craddock and Maxwell, 1993; Carr, 1996; Maxwell and Craddock, 1995; Grant, 2000; Craddock and Howard, 2002; Grant and Parker, 2002). Carr (1995, 1996) attempted to explain formation of valley networks by groundwater sapping combined with mass wasting induced by surface runoff, such as by collapse of surface material by fluvial undercutting or incorporation of water into surficial material to form wet debris flows. However, in the map area, variations in valley widths and depths along the lengths of the valleys, which are uncharacteristic of sapping valleys, and several valleys that head near crater rim crests suggest that a significant component of surface runoff was not derived from ground water but from direct precipitation or melting snow or ice. This scenario has also been proposed for the Margaritifer Sinus area (MC-16 quadrangle; Grant, 2000; Grant and Parker, 2002) and for other areas within the Martian highlands (Craddock and Maxwell, 1993; Maxwell and Craddock, 1995; Craddock and Howard, 2002). Studies of the extensive, integrated drainage system of Vichada Valles provide additional information that may be used to interpret the styles of fluvial activity that shaped the Martian highlands. Although high-resolution imaging datasets allowed identification of small tributaries not observed earlier (Carr, 1995, 1996), there are still large undissected interfluve regions within the highlands surrounding Vichada Valles. Formation of a drainage system of this magnitude and morphology would require either (1) mobilization of volatiles contained within an extensive subsurface reservoir or (2) widespread precipitation. High infiltration rates presumably characterize the surface and near-surface material and the formation of valley segments likely includes a combination of sapping and runoff processes; larger valley segments would be formed in runoff-dominated phases or as greater volumes of groundwater collected in the surface drainage system.

During the Late Noachian and Early Hesperian Epochs, impact craters were degraded as well. In addition to eroded ejecta blankets and rims, impact craters in the map area show interior walls incised by numerous gullies and floors containing deposits of relatively smooth fill material. Millochau is a good example of a crater where detailed analysis and mapping of the floor deposits could be accomplished using available MOC and THEMIS images (Mest and Crown, 2005). Millochau floor deposits display surface textures similar to those of the intercrater plains material, containing degraded pits and craters and low-lying areas filled with darker sediments. The geology of Millochau is complex, revealing a history of emplacement of sequences of sedimentary, volcanic, and (or) impact materials that subsequently experienced degradation, possibly involving collapse and fluvial erosion. Sedimentation within Millochau appears to be related, in part, to erosion of the interior crater rim by numerous gullies but may also include contributions from eolian and lacustrine activity (Mest and Crown, 2005). Although the unit areas within Millochau are small, which produces rather large uncertainties in their unit ages, Okotoks in western Millochau displays a fairly unmodified ejecta blanket with relatively large area. Crater size-frequency distributions for the Okotoks ejecta provide upper age constraints of middle to Upper Hesperian for the emplacement and erosion of the Millochau interior deposits and the central plateau (Mest and Crown, 2005). Crater size-frequency distributions and superposition relations indicate emplacement, and most of the erosion of Millochau floor deposits occurred prior to formation of Okotoks within a period ranging from Middle Noachian to Upper Hesperian. Although Millochau is the only crater in the map area that has been imaged in such detail, other large craters contain similar floor deposits that may have similar histories.

Emplacement of the smooth plateau unit (Hpl_3) in the southeast corner of the map area, as well as deposition and remobilization of valley floor material, also took place during the Late Noachian and Early Hesperian. Valley floor material probably consists of material eroded from the highlands and deposited in the channels via fluvial and eolian processes and shows dune forms in high-resolution MOC images, suggesting that it is composed of easily mobilized material. Eolian transport and deposition of material also occurred in the southernmost exposures of the intercrater plains material. The plains material in this part of the map area is subdued. MOC images show that high-standing outcrops of the pitted and degraded material, characteristic of the plains in the northern part of the map area, are surrounded by smooth, darker material that fills low-lying areas of the plains and forms dune features. Dark material and dune features are also found on the high-standing outcrops of the intercrater plains material, but the overall pitted and irregular surfaces characteristic of the plains are visible through this material, suggesting the mantling layer is relatively thin. Sources of this fine-grained sediment could include material deposited by the valley networks that characterize the area, ejecta of several large and relatively young impact craters, and eolian material from Hellas Planitia and the surrounding highlands. Except for Millochau and valley floors, well-developed dune fields seen in MOC images are only found in the southern part of the map area.

The most recent activity in the map area involves eolian processes that formed the dune material in Millochau and in the valley floor material, eroded the uppermost layers of the intercrater plains, and redistributed material throughout the map area. Some of this activity may be geologically recent and

currently active. Also, mass wasting processes, such as formation of talus deposits, in Millochau and other large craters appear to be geologically recent, although their surfaces may reflect younger modification.

Investigations of highland degradation in this and other areas of the highlands surrounding Hellas Planitia provide important insights into the potential variability of geologic processes and climatic conditions. For comparison, geologic mapping on the east rim of Hellas Planitia (Crown and others, 1992; Mest and Crown, 2001b, 2002b, 2003) shows that much of the fluvial activity is younger than similar activity in Tyrrhena Terra. Valley networks in the highlands adjacent to Reull Vallis (MC–28 quadrangle) formed in the middle to Late Hesperian, because they dissect Late Noachian to Early Hesperian intermontane sedimentary deposits; these networks probably contributed sediments to the adjacent plains material that is Early to middle Hesperian in age. These valley networks are an order of magnitude smaller in scale than those in Tyrrhena Terra and tend to be confined to low-lying areas among highland massifs. The large events that formed Reull Vallis also most likely occurred in the Hesperian; this type of activity is not observed in the Tyrrhena Terra area. In addition to the evidence for fluvial processes, the highlands east of Hellas contain numerous Amazonian debris aprons formed by downslope movement of volatile-rich debris (Crown and others, 1992; Crown and Stewart, 1995; Mest and Crown, 2001b, 2002b, 2003; Pierce and Crown, 2003). The significant differences between the ages, scales, and morphologies of fluvially produced features suggest that (1) the climate histories of Tyrrhena Terra and Reull Vallis differ significantly, (2) the distribution of volatiles around Hellas Planitia varies greatly, even within a few hundred kilometers, and (or) (3) the effects of fluvial processes on the landscape were greatly dissimilar in the two areas. MOLA and THEMIS data used in conjunction with geologic mapping will enable the styles and timing of degradational processes to be determined. Specifically, watershed modeling will further constrain fluvial activity in these highland terrains (Mest, 2004; Mest, unpub. data, 2006).

ACKNOWLEDGEMENTS

The authors wish to thank Tracy Gregg, Ken Herkenhoff, and Ken Tanaka for their insightful reviews. Helpful comments on an early version of this work, specifically regarding Millochau crater, were provided by Edmond Grin and James Head. This project was supported by NASA grant NAG5-10529 from the Planetary Geology and Geophyisics Program. This is Planetary Science Institute (PSI) Contribution 405.

REFERENCES CITED

Arvidson, R.E., Boyce, J.M., Chapman, C.R., and 9 others, 1979, Standard techniques for presentation and analysis of crater size-frequency data: Icarus, v. 37, p. 467–474.

Carr, M.H., 1995, The Martian drainage system and the origin of valley networks and fretted channels: Journal of Geophysical Research, v. 100, p. 7479–7507.

Carr, M.H., 1996, Water on Mars: New York, Oxford University Press, 229 p.

Christensen, P.R., Bandfield, J.L., Hamilton, V.E., and 23 others, 2001, The Mars Global Surveyor Thermal Emission Spectrometer experiment—Investigation description and surface science results: Journal of Geophysical Research, v. 106, p. 23,823–23,871.

Craddock, R.A., and Howard, A.D., 2002, The case for rainfall on a warm, wet early Mars: Journal of Geophysical Research, v. 107 (doi:10.1029/2001JE001505).

Craddock, R.A., and Maxwell, T.A., 1993, Geomorphic evolution of the Martian highlands through ancient fluvial processes: Journal of Geophysical Research, v. 98, p. 3453–3468.

Crown, D.A., and Greeley, Ronald, 1993, Volcanic geology of Hadriaca Patera and the eastern Hellas region of Mars: Journal of Geophysical Research, v. 98, p. 3431–3451.

Crown, D.A., and Greeley, Ronald, in press, Geologic map of MTM –30262 and –30267 quadrangles, Hadriaca Patera region of Mars: U.S. Geological Survey Scientific Investigations Map 2936, scale 1:1,000,000.

Crown, D.A., Price, K.H., and Greeley, Ronald, 1992, Geologic evolution of the east rim of the Hellas basin, Mars: Icarus, v. 100, p. 1–25.

Crown, D.A., and Stewart, K.H., 1995, Debris aprons in the eastern Hellas region of Mars, *in* Lunar and Planetary Science Conference, XXVI: Houston, Tex., Lunar and Planetary Institute, p. 301–302.

Edgett, K.S., 2001a, Geologic aspects and relations of small eolian dunes and large ripples on Mars [abs.], *in* Lunar and Planetary Science Conference, XXXII: Houston, Tex., Lunar and Planetary Institute, no. 1181 [CD-ROM].

Edgett, K.S., 2001b, Observations regarding small eolian dunes and large ripples on Mars [abs.]: Geological Society of America, Abstracts with Programs, v. 33, no. 19,777.

Fagin, S.W., Worrall, D.M., and Muehlberger, W.R., 1978, Lunar mare ridges orientations—Implications for lunar tectonic models, *in* Proceedings of the Lunar and Planetary Science Conference, 9th: Houston, Tex., Lunar and Planetary Institute, p. 3473–3479.

Frey, H.V., Hutchison, Leah, Sakimoto, S.E.H., and Roark, J.H., 2000, A large population of possible buried impact basins on Mars revealed by MOLA topographic data [abs.], *in* Lunar and Planetary Science Conference, XXXI: Houston, Tex., Lunar and Planetary Institute, no. 1736 [CD-ROM].

Goldspiel, J.M., and Squyres, S.W., 2000, Groundwater sapping and valley formation on Mars: Icarus, v. 148, p. 176–192.

Goldspiel, J.M., Squyres, S.W., and Jankowski, D.G., 1993, Topography of small Martian valleys: Icarus, v. 105, p. 479–500.

Grant, J.A., 1999, Evaluating the evolution of process specific degradation signatures around impact craters: International Journal of Impact Engineering, v. 23, p. 331–340.

Grant, J.A., 2000, Valley formation in Margaritifer Sinus, Mars, by precipitation-recharged ground-water sapping:

Geology, v. 28, p. 223–226.
Grant, J.A., and Parker, T.J., 2002, Drainage evolution in the Margaritifer Sinus region, Mars: Journal of Geophysical Research, v. 107 (doi:10.1029/2001JE001678).
Grant, J.A., and Schultz, P.H., 1993, Degradation of selected terrestrial and Martian impact craters: Journal of Geophysical Research, v. 98, p. 11,025–11,042.
Grant, J.A., and Schultz, P.H., 1994, Early fluvial degradation in Terra Tyrrhena, Mars—Constraints from styles of crater degradation on the Earth, *in* Lunar and Planetary Science Conference, XXV: Houston, Tex., Lunar and Planetary Institute, p. 457–458.
Greeley, Ronald, and Crown, D.A., 1990, Volcanic geology of Tyrrhena Patera, Mars: Journal of Geophysical Research, v. 95, p. 7133–7149.
Greeley, Ronald, and Guest, J.E., 1987, Geologic map of the eastern equatorial region of Mars: U.S. Geological Survey Miscellaneous Investigations Series I–1802B, scale 1:15,000,000.
Greeley, Ronald, and Spudis, P.D., 1981, Volcanism on Mars: Reviews of Geophysics, v. 19, p. 13–41.
Gregg, T.K.P., Crown, D.A., and Greeley, Ronald, 1998, Geologic map of the Tyrrhena Patera region of Mars (MTM quadrangle –20252): U.S. Geological Survey Miscellaneous Investigations Series Map I–2556, scale 1:500,000.
Jakosky, B.M., Mellon, M.T., Kieffer, H.H., Christensen, P.R., Varnes, E.S., and Lee, S.W., 2000, The thermal inertia of Mars from the Mars Global Surveyor Thermal Emission Spectrometer: Journal of Geophysical Research, v. 105, p. 9643–9652.
Leonard, G.J., and Tanaka, K.L., 2001, Geologic map of the Hellas region of Mars: U.S. Geological Survey Geologic Investigations Series I–2694, scale 1:5,000,000.
Lucchitta, B.K., 1976, Mare ridges and related highland scarps—Results of vertical tectonism?, *in* Proceedings of the Lunar and Planetary Science Conference, 7th: Houston, Tex., Lunar and Planetary Institute, p. 2761–2782.
Maxwell, T.A., and Craddock, R.A., 1995, Age relations of Martian highland drainage basins: Journal of Geophysical Research, v. 100, p. 11,765–11,780.
Mellon, M.T., Jakosky, B.M., Kieffer, H.H., and Christensen, P.R., 2000, High-resolution thermal inertia mapping from the Mars Global Surveyor Thermal Emission Spectrometer: Icarus, v. 148, p. 437–455.
Mest, S.C., 2004, Evolution of the martian highlands: Implications from drainage basin characteristics and valley network morphologies: Penn., University of Pittsburgh, Ph.D. Dissertation, 294 p.
Mest, S.C., and Crown, D.A., 2001a, Fluvial degradation of the circum-Hellas highlands of Mars [abs.], *in* Field trip and workshop on the Martian Highlands and Mojave Desert analogs, October 20–27, 2001, Las Vegas, Nev. and Barstow, Calif.: Houston, Tex., Lunar and Planetary Institute, no. 4014.
Mest, S.C., and Crown, D.A., 2001b, Geology of the Reull Vallis Region, Mars: Icarus, v. 153, p. 89–110.
Mest, S.C., and Crown, D.A., 2002a, Geology of MTM quadrangles –20272 and –25272, Terra Tyrrhena region of Mars [abs.], *in* Lunar and Planetary Science Conference, XXXIII: Houston, Tex., Lunar and Planetary Institute, no. 1730 (CD-ROM).
Mest, S.C., and Crown, D.A., 2002b, Geologic map of MTM –40252 and –40257 quadrangles, Reull Vallis region of Mars: U.S. Geological Survey Geologic Investigations Series I–2730, scale 1:1,000,000.
Mest, S.C., and Crown, D.A., 2003, Geologic map of MTM –45252 and –45257 quadrangles, Reull Vallis region of Mars: U.S. Geological Survey Geologic Investigations Series I–2763, scale 1:1,000,000.
Mest, S.C., and Crown, D.A., 2005, Millochau crater, Mars—Infilling and erosion of an ancient highland impact crater: Icarus, I08883.
Mest, S.C., Crown D.A., and Harbert, William, 2002, Fluvial degradation of the highlands—The Terra Tyrrhena region of Mars [abs.], *in* Lunar and Planetary Science Conference, XXXIII: Houston, Tex., Lunar and Planetary Institute, no. 1892 (CD-ROM).
Murray, B.C., Soderblom, L.A., Sharp, R.P., and Cutts, J.A., 1971, The surface of Mars, 1. Cratered terrains: Journal of Geophysical Research, v. 76, p. 313–330.
Phillips, R.J., and Lambeck, Kurt, 1980, Gravity fields of the terrestrial planets—Long-wavelength anomalies and tectonics: Reviews of Geophysics and Space Physics, v, 18, p. 27–76.
Pierce, T.L., and Crown, D.A., 2003, Morphologic and topographic analyses of debris aprons in the eastern Hellas region, Mars: Icarus, v. 163, p. 46–65.
Pike, R.J., and Spudis, P.D., 1987, Basin-ring spacing on the Moon, Mercury, and Mars—Earth, Moon, and Planets, v. 39, p. 129–194.
Putzig, N.E., Mellon, M.T., and Arvidson, R.E., 2003, Thermophysical properties of the martian south polar region [abs.], *in* Sixth International Conference on Mars: Houston, Tex., Lunar and Planetary Institute, no. 3173.
Roark, J.H., and Frey, H.V., 2001, GRIDVIEW: Recent improvements in research and education software for exploring Mars topography [abs.], *in* Lunar and Planetary Science Conference, XXXII: Houston, Tex., Lunar and Planetary Institute, no. 1618 (CD-ROM).
Roark, J.H., Frey, H.V., and Sakimoto, S.E.H., 2000, Interactive graphics tools for analysis of MOLA and other data [abs.], *in* Lunar and Planetary Science Conference, XXXI: Houston, Tex., Lunar and Planetary Institute, no. 2026 [CD-ROM].
Schaber, G.G., 1977, Geologic map of the Iapygia quadrangle, Mars: U.S. Geological Survey Miscellaneous Investigations Map I–1020, scale 1:5,000,000.
Scott, D.H., and Tanaka, K.L., 1986, Geologic map of the western equatorial region of Mars: U.S. Geological Survey Miscellaneous Investigations Map I–1802A, scale 1:15,000,000.
Strom, R.G., 1972, Lunar mare ridges, rings, and volcanic ring complexes: Modern Geology, v 2, p. 133–157.

Tanaka, K.L., 1986, The stratigraphy of Mars, *in* Proceedings of the Lunar and Planetary Science Conference, 17th: Journal of Geophysical Research Supplement, v. 91, p. E139–E158.

Tanaka, K.L., Isbell, N.K., Scott, D.H., Greeley, Ronald, and Guest, J.E., 1988, The resurfacing history of Mars: A synthesis of digitized, Viking-based geology, *in* Proceedings of the Lunar and Planetary Science Conference, 18th: Houston, Tex., Lunar and Planetary Institute, p. 665–678.

Tanaka, K.L., and Leonard, G.J., 1995, Geology and landscape evolution of the Hellas region of Mars: Journal of Geophysical Research, v. 100, p. 5407–5432.

Tanaka, K.L., Scott, D.H., and Greeley, Ronald, 1992, Global stratigraphy, *in* Kieffer, H.H., Jakosky, B.M., Snyder, C.W., and Matthews, M.S., eds., Mars: Tucson, University of Arizona Press, p. 345–382.

Tanaka, K.L., Skinner, J.A., and Hare, T.M., 2005, Geologic Map of the northern plains of Mars: U.S. Geological Survey Scientific Investigations Map 2888, scale 1:15,000,000.

Wood, C.A., 1980, Martian double ring basins—New observations, *in* Proceedings of the Lunar and Planetary Science Conference, 11th: Houston, Tex., Lunar and Planetary Institute, p. 2221–2241.

Table 1. *Crater size-frequency data and unit ages*

[Craters counted within Mars Transverse Mercator (MTM) –20272 and –25272 quadrangles[1]. Areas equal total unit exposures within this map area. N(2), N(5), and N(16) represent the cumulative number of craters >2, >5, and >16 km in diameter/10^6 km^2. Error = ± [(N1/2)/A] x 10^6 km^2, where A is area (Arvidson and others, 1979). Crater count age ranges are based upon crater-density boundaries determined by Tanaka (1986): MA, Middle Amazonian; EA, Early Amazonian; LH, Late Hesperian; EH, Early Hesperian; LN, Late Noachian; MN, Middle Noachian; EN, Early Noachian. Unit age is based upon superposition and crosscutting relations and crater counts. See Description of Map Units for names of geologic units]

Unit label	Total craters[2] <2 km diam	Total craters >2 km diam	Total (km^2)	N(2)	N(5)	N(16)	Crater count age range	Unit age
AHt	96	2	956	2,091±1,479	0	0	LN-LH	LH or younger
HNvf	46	12	2,533	4,738±1,368	1,974±883	1,184±684	EN-LH	LN or younger
Hpl_3	9	4	1,022	3,915±1,958	2,937±1,695	2,937±1,695	MN-LN	EH-LH
Npi	532	181	60,124	3,011±224	1,663±166	699±108	EN-LN	MN-LN
Nm	4	1	466	2,147±2,147	0	0	MN-EA	EN-MN
Amd	40	0	154	0	0	0	EH-MA	EA or younger
HNme	149	2	462	4,329±3,061	2,164±2,164	0	MN-EA	MN-LH
HNmr	799	4	3,400	1,177±588	833±510	294±294	EN-LH	MN-LH
Nmp	1,603	3	1.160	2,586±1,493	1,724±1,219	862±862	EN-EH	MN-LN
Millochau floor[3]	2,545	7	5,130	1,365±516	585±338	195±195	EN-EH	--[3]
Millochau floor	380	19	5,494	3,458±793	1,456±515	182±182	EN-EH	--[4]
HNcf	86	8	13,803	580±205	217±126	72±72	MN-LH	MN-LH
c_3	126	16	14,056	1,138±285	285±142	71±71	MN-EH	EH or younger
c_2	23	5	1,472	3,397±1,519	1,359±961	0	MN-EH	MN-EH
c_1	11	6	2,033	2,951±1,205	1,968±984	1,476±852	EN-LN	EN-LN

[1]The entire floor of Millochau crater was mapped (Mest and Crown, 2005), portions of which are located beyond the western boundary of the map area.

[2]Includes craters >0.5 km diam counted for Hpl_3, HNvf, HNcf, Npi, and Nm and craters >0.05 km diam counted for AHt and Millochau units (Amd, HNme, HNmr, Nmp).

[3]Includes areas and counts for all units composing the Millochau floor assemblage (Nmp, pitted; HNmr, rugged; HNme, etched; Amd, dune materials; see Mest and Crown, 2005). Unit age not determined for the floor as a whole; crater size-frequency data shown for comparison only with unit HNcf.

[4]Unit age not determined for Millochau rim materials; crater size-frequency data shown only for comparison with units c_3, c_2 and c_1.